

Structure and Dynamics of Spontaneous and Induced ELMs on ASDEX Upgrade

J. Neuhauser, V. Bobkov, G. D. Conway, R. Dux, T. Eich, M. Garcia-Munoz, A. Herrmann, L. Horton, A. Kallenbach, S. Kalvin², B. Koch¹, G. Kocsis², B. Kurzan, P. Lang, M. Maraschek, H. W. Mueller, H. D. Murmann, R. Neu, M. Reich, V. Rohde, A. Schmid, W. Suttrop, M. Tsalas³, E. Wolfrum and the ASDEX Upgrade Team

Max-Planck-Institut fuer Plasmaphysik, EURATOM Association, Garching, Germany

1 Humboldt University, Berlin, Germany

2 KFKI-RMKI, EURATOM Association, Budapest, Hungary

3 NCRS Demokritos, EURATOM Association, Athens, Greece

e-mail: Josef.Neuhauser@ipp.mpg.de

Abstract. In order to assess the contribution of edge localized modes (ELMs) to plasma-wall interaction in future fusion experiments like ITER, a sound experimental data basis for model validation and extrapolation, and, to be prepared for the unfavourable case, the development of tools for ELM mitigation are required. On ASDEX Upgrade, exploiting the fast edge/divertor diagnostics as well as active ELM control tools, especially ELM pacing by cryogenic pellet injection, a large amount of experimental information has been accumulated on the structure and dynamics of natural and induced ELMs, as well as on related wall effects. In this paper, a survey of ELM structure related diagnostics and results is given first. Recent progress in spontaneous ELM analysis is given then with emphasis on magnetic probe analysis, 2d Thomson scattering snapshots of pedestal density and temperature perturbations in comparison with electron cyclotron emission, and combined Langmuir, magnetic and thermographic investigation of filament dynamics in the scrape-off layer wing. Pellet induced ELMs are characterized in comparison to spontaneous ones. The combined experimental evidence is finally discussed in terms of simple considerations based on presently available, still rudimentary models.

1. Introduction

In present day high-confinement (H-mode) divertor tokamak operation, a significant part of plasma-wall interaction is due to edge localized modes (ELMs), releasing a substantial amount of particles and energy to first wall and divertor in a burst-like fashion. Simple empirical extrapolation of the most dangerous type-I ELMs to the forthcoming ITER indicates possibly intolerable power load and material erosion on divertor targets and even on main chamber wall elements [1]. A more quantitative assessment requires a sound experimental data basis for model validation and extrapolation, and, to be prepared for the unfavourable case, the development of tools for ELM control e.g. via external ELM pacing. The latter must include the characterization of the externally induced ELMs in comparison to spontaneous ones. Since ELMs consist of a burst of extremely fast three-dimensional, highly non-linear helical instabilities, a detailed analysis of the ELM structure, evolution and resulting wall load is a crucial ingredient for physical understanding and extrapolation to future devices. On ASDEX Upgrade, exploiting the extensive set of fast edge diagnostics, a large amount of information has been and is being accumulated on global ELM characteristics as well as on detailed ELM structures [2,3]. In addition, several techniques for ELM pacing and mitigation have been tested, the most successful one relying on quasi-continuous cryogenic pellet injection [4]. In fact, the latter has even been routinely applied in radiative edge discharge scenarios to enforce regular ELMs, preventing impurity penetration and accumulation in between ELMs [5]. In this paper, a short overview of ELM diagnostics and main results is given first. Recent advances in ELM structure analysis, primarily of spontaneous ELMs, are then described in more detail, followed by a characterization of pellet triggered ELMs as compared to spontaneous ones. The combined results are finally discussed in the light of theoretical ELM models.

2. Survey of ELM related diagnostics and spontaneous ELM results

In figure 1, a poloidal ASDEX Upgrade cross section is shown together with the approximate positions of a selection of fast diagnostics used for ELM investigations.

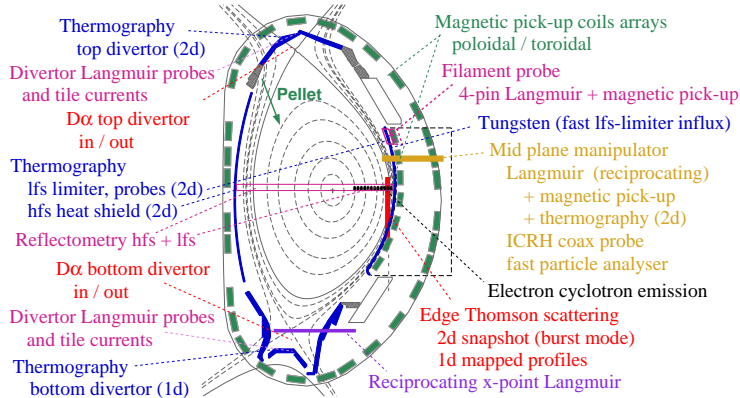


FIG.1. Poloidal cross section of ASDEX Upgrade together with an upper single null equilibrium, the positions of a selection of fast ELM related diagnostics and the pellet injection path.

Of course, a comprehensive overview of related measurements is far beyond the scope of this paper. Therefore, in this section, we focus on those results contributing to ELM structure analysis in substantial detail. As we shall see, for pedestal and hot scrape-off layer (sol) mode analysis, these are mainly edge Thomson scattering [6,7], reflectometry [8,9], electron cyclotron emission [10] and the poloidal-toroidal magnetic pick-up coil arrays (to be described in the next section). In contrast, sol filaments and wall load pattern are best analysed by a combination of various Langmuir probes and thermographic cameras [11-16] and to some extent again Thomson scattering [7] and magnetic probes [14].

Starting with power deposition on first wall elements, a key result was the discovery of non-axisymmetric spiral structures on top divertor target plates, interpreted as footprints of detached helical filaments in the sol [15,16]. Toroidal quasi-mode numbers (events on a toroidal circumference) of about 8-24 were derived, with the low values preferentially in the initial ELM phase. The transient ELM power load pattern on low field side (lfs) limiters gave similar or even higher values [13]. Reciprocating Langmuir probe scans in the sol, moving either the probe or the plasma, provided information on filament source rate, velocity, radial decay etc [12-14] (see also next section for recent progress). Strong perturbations in pedestal (holes) and hot sol (blobs) have been discovered recently on 2d Thomson scattering snapshots during ELMs, but surprisingly also in between [6,17]. These are nearly invisible on magnetic pick-up coils, but obvious on electron cyclotron emission as reported in the next section. We should mention that spiky inter-ELM and ELM precursor events (up to mini-ELMs already visible on divertor D_{α}) are frequently observed even far out in the limiter shadow on Langmuir probes [11] and, even more clearly, on a dedicated ion cyclotron frequency arcing probe [18]. This might indicate that the local inter-ELM edge gradients transiently approach stability limits with respect to filament or ELM growth.

3. Recent progress in spontaneous ELM analysis: Selected topics

3.1 ELM structure and time evolution detected by magnetic probe arrays

In ASDEX Upgrade, there are essentially two types of magnetic pick-up coils and coil arrays, each with 2 MHz sampling, measuring dB_r/dt ('BAL probes') and dB_{θ}/dt ('Mirnov

coils'), respectively, which together allow determination of the spatial ELM structure up to intermediate toroidal mode numbers. A third poloidal BAL-array with double spatial resolution (twice the n-limit) and 2.5 MHz sampling is focused on frequencies above 100 kHz, but limited to a 400 ms interval per discharge.

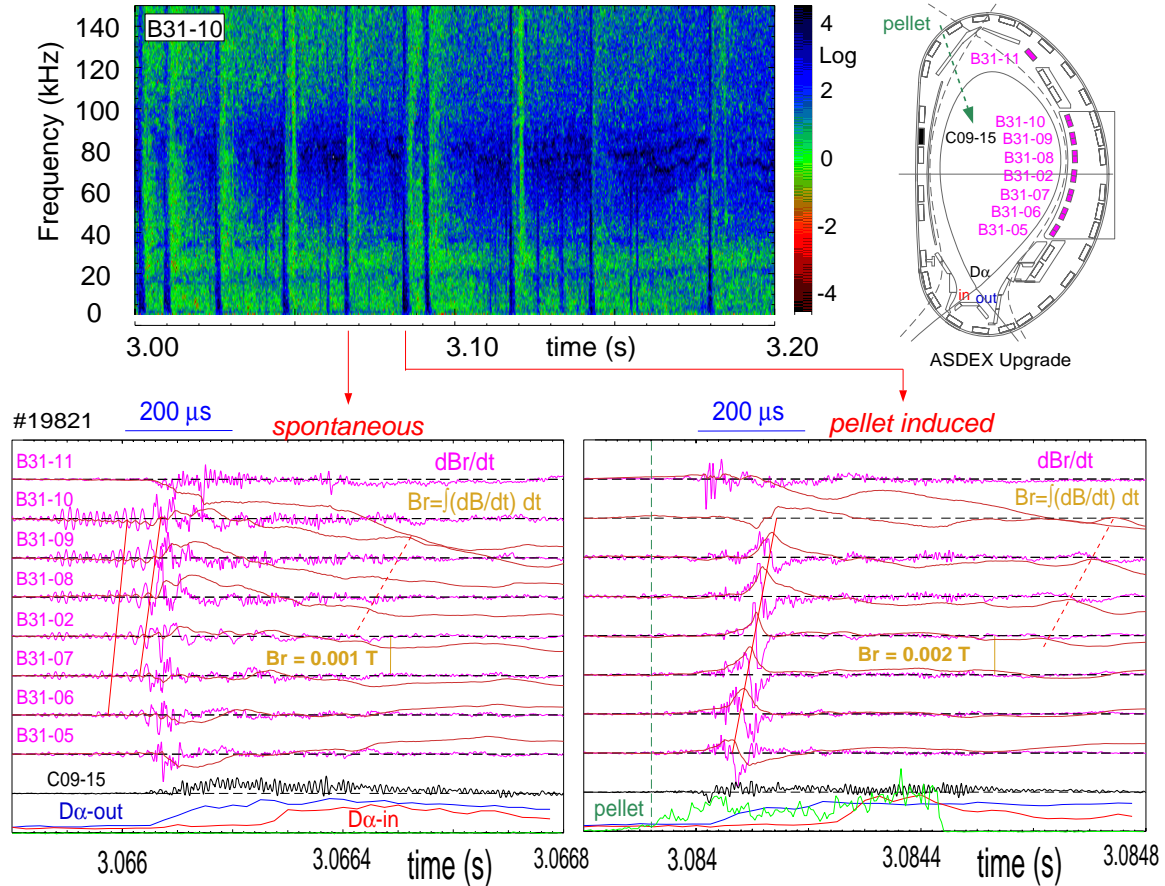


FIG. 2. Top: Spectrogram of a selected magnetic pick-up coil of shot #19821, together with an insert indicating probe positions and the pellet injection path. Bottom: dB/dt traces of eight low field side and one high field side probes in comparison with inner/outer divertor D_α and the pellet ablation monitor (left: spontaneous ELM, right: pellet triggered ELM).

As an example, figure 2 shows typical magnetic data for #19821, a discharge tailored for perturbative ELM pacing ($B_t = 2.7$ T, $I_p = 1$ MA, $q_{95} = 4.9$, $n = 6 \cdot 10^{19} \text{ m}^{-3}$, $P_{NI} = 5$ MW). On top, a spectrogram of a selected BAL probe is given for a 200ms window containing a bunch of spontaneous ELMs (appearing as broadband vertical lines), and one triggered by a single pellet injected at $t = 3.084$ s. In between ELMs there is a clear quasi-coherent mode activity especially between 60 and 100 kHz, growing shortly after an ELM and lasting until the next one. Magnetic probe analysis reveals a helical, field aligned mode structure with toroidal mode number around $n = 8$, rotating upward at lfs, i.e. in the electron drift direction (and the pedestal ExB direction). These modes are reminiscent of the washboard modes observed in JET [19]. In the bottom part, time traces are shown over a 1ms window each, on the right side for the pellet triggered ELM (to be discussed in section 4) and, on the left, for the preceding spontaneous ELM. The magenta lines show the $dB/dt(t)$ signals from a lfs poloidal BAL array and the orange ones give the respective integrals, $B_r(t)$ (with B_r set to zero at the window start; absolute B_r -scale indicated). In addition, one high field side (hfs) Mirnov coil

signal dB/dt and the D_α emission from inner/outer divertor and from the ablating pellet, if present, are shown (see insert top/right for poloidal diagnostic locations and the pellet path). Focusing on the spontaneous ELM traces, we see initially the washboard-type precursor mode with maximum amplitude above mid plane (where the actual equilibrium is closest to the probe array), apparently growing and slightly slowing down in frequency, forming the dominant structure in the first ELM phase. Notice that this initial mode is nearly invisible on the top and hfs probes, indicating a dominant lfs ballooning structure. Several additional higher frequency perturbations (e.g. around 140kHz), interfering with each other, appear then on the lfs dB_r/dt , partly also on hfs (e.g. ~ 90 kHz), but are smoothed away on B_r . In parallel the outer divertor D_α starts to rise. One should notice that it is B_r which characterizes the spatial mode amplitude. To get a rough estimate, we assume a parallel wave number $k_{\parallel} \sim 1/(qR)$ typical for a lfs ballooning mode. Together with the experimental $B_r/B \sim 10^{-4}$ at the probe position and $\sim 10^{-3}$ extrapolated to the pedestal radius (with $n \sim 8$ or, equivalent, $k_\theta \sim 20/\text{m}$ on lfs mid plane), we get radial mode amplitudes of a fraction of a centimeter, smaller than, but comparable to the pedestal width. The $B_r(t)$ evolution on a several 100 microsecond scale and beyond is partly due to equilibrium shift ($n=0$), but the toroidally distributed (non-equidistant) mid plane probes still indicate strong toroidal variations. The corresponding mode mix is still to be analysed. The latter is much more difficult for these transient ELM structures (with rather short correlation lengths and times) than for continuous, coherent modes, where rotation can be exploited for accurate mode reconstruction even with a small number of properly distributed probes.

Having described one specific ELM, the question is how general the features are. In fact, ELMs in similar medium power shot scenarios and even within the same shot phase vary substantially in detail. Looking at discharges with much higher heating power, e.g. #18713 ($B_t = 2.3$ T, $I_p = 1$ MW, $P_{\text{NI}} = 10$ MW) designed for neoclassical tearing mode investigation, or #20176 ($B_t = 2.1$ T, $I_p = 0.8$ MW, $P_{\text{NI}} = 10$ MW, $P_{\text{ICRH}} = 2$ MW), an improved H-mode discharge, the ELM analysis is more difficult because of strong core modes and their harmonics. Qualitatively, ELMs in #18713 are similar to those above, though with less high frequency turbulence. ELMs in shot #20176 are clearly more complicated. In addition to several core modes, the spectrograms show a lot of broadband inter-ELM activity, and a washboard-type mode pattern between 100 and 180 kHz. The ELMs show initially some low-n/low frequency structure moving upward as usual. In addition, especially after the maximum of the divertor D_α emission (with the pedestal already partially eroded), an intense, fairly coherent mode appears near 100 kHz with $n=4$, disappearing again after the ELM. Surprisingly, the rotation of this mode is poloidally downwards (ion drift direction), in contrast to all cases before.

3.2 Thomson scattering analysis of edge-pedestal mode structures

In standard operation, the multi-pulse edge Thomson scattering system is run in quasi-continuous mode, and electron temperature T_e and density n_e in the respective scattering volumes are mapped onto a 1d radial coordinate. These profiles show a significant data scatter beyond statistical noise, which has been attributed to local filamentary structures appearing as outliers on an average 1d profile [7]. In fact, exploiting the 2d arrangement of scattering volumes, and running the radially staggered, vertical laser beams in burst mode within 2.5 microseconds, one gets 2d snapshots revealing holes in the pedestal and blobs in the scrape-off layer during ELMs, but also in between, corresponding to estimated toroidal wave numbers of $n = 8-20$ [6]. Surprisingly, apart from a slowly moving structure in the

poloidal B_r pattern (measured five sectors away in counter current direction), no clearly correlated magnetic signature could be identified, suggesting that these perturbation might be due to nearly locked modes.

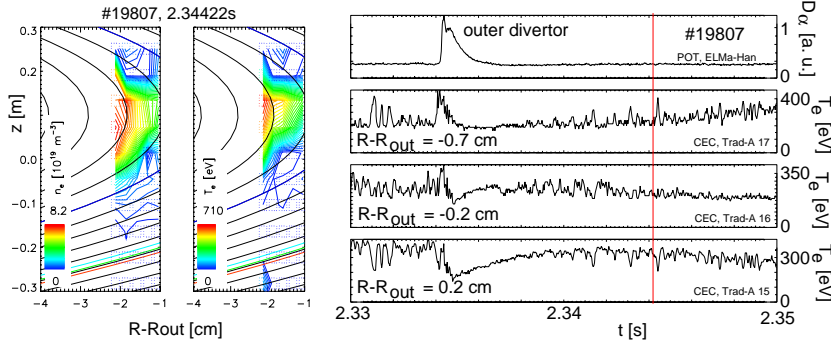


FIG. 3. Left: 2d poloidal density and temperature snapshots of shot #19807s. Right: Apparent electron temperature from ECE at three radii in comparison with divertor D_α (snapshot time indicated by vertical line).

Recently, a comparison between 2d snapshots and electron cyclotron emission (32 kHz sampling; six sectors away in co-direction) has identified discharges, which clearly show repeated transient mode structures in the pedestal for the same time interval where the 2d snapshots see pedestal modes. This is demonstrated in figure 3, where 2d density and temperature contour plots from the Thomson array (left) are given as well as the electron cyclotron 'temperature' evolution on three edge/pedestal channels (right; snapshot time marked by a vertical line). In addition to the ELM crash, a lot of randomly distributed events are observed in between ELMs with a phase inversion in the steep gradient region. The latter might indicate slowly rotating helical magnetic island remnants in the steep gradient region, though possible artefacts related to decreasing optical thickness towards the separatrix remain to be checked. Recently, about 527 snapshots from shots #20414-20420 have been analysed. About 60 % showed sufficiently clear structures to derive an approximate toroidal quasi-mode-number, typically in the range $n = 6 - 50$, surprisingly without drastic difference between ELM and inter-ELM phases [17].

3.3 ELM structure and filament analysis in the scrape-off layer

For a limited number of shots, the mid plane manipulator, equipped with a multi-pin Langmuir head and/or magnetic pick-up coils, has been used to investigate the ELM induced filament structure and dynamics in the scrape-off layer wing and limiter vicinity [12,13]. More recently, a specific 'filament probe' has been implemented near the manipulator on approximately the same magnetic flux bundle [14]. It combines a BAL-type magnetic probe with four Langmuir pins at the front and can be shifted on purpose out of the limiter shadow to investigate plasma filaments just in front of the limiter. In addition, a 2d thermography camera viewing these probes and adjacent limiters is used to derive the heat load onto these elements. The distance between probes and plasma is substantially varied by radial plasma position scans. Figure 4 shows probe details and their position in the torus (right) together with the radial heat flux decay (left) from thermography and the two Langmuir heads as function of the distance between separatrix and reciprocating probe. Somewhat arbitrarily, $\gamma Te = 100$ eV per electron-ion pair has been assumed to convert the measured ion saturation current into a power scale [14]. The points refer to maximum values measured for individual filaments. The essence here is that particle and power flux have nearly identical decay lengths, leaving little freedom for interpretation in terms of parallel loss modeling of radially drifting filaments (e.g. ion temperature well above electron temperature). The absolute difference between both Langmuir probes lines is explained by their different radial position (about one e-folding length). Correlating the four pins of the filament probe yields a

downward cross-field velocity of a few km/s, filament heights of several centimeters and substructure down to a few millimeters. An attempt to model the magnetic signal in the nearby integrated pick-up coil by a dipole current in these 'open' filaments according to simple models [20] reproduced some qualitative features, but the required currents were by one to two orders of magnitude higher than the filament ion saturation current. Therefore the magnetic signals are most likely due to 'attached' mode structures in the pedestal as discussed in section 3.1.

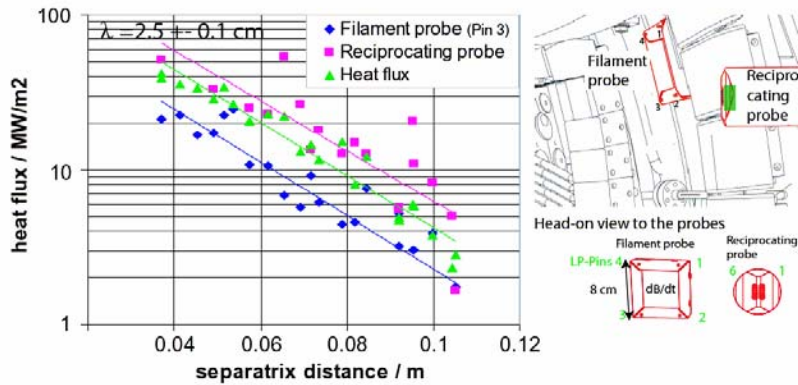


FIG. 4. Radial decay of heat fluxes derived from Langmuir probes and thermography (viewing these probes) as function of distance between separatrix and reciprocating probe head. The probe geometry is indicated also (3d and front view).

4. Pellet induced versus spontaneous ELMs

As mentioned in the introduction, ELM pacing by pellets is a viable option for future machines to mitigate ELMs or, possibly more importantly, to sustain an optimum ELM frequency, e.g. in radiating edge discharges, to avoid ELM free phases and radiation collapse [5]. Accordingly, the question is if and how triggered ELMs differ from spontaneous ones. Applied in a perturbative way (pellet rate much smaller than ELM frequency), small and shallow pellet injection may also be seen as a tool to investigate pedestal stability, time scales for communication from the seed perturbation around the torus, non-linear mode growth and filament ejection [21,22]. For the present analysis, the hfs pellet injection system is used with velocities between 240 and 1000 m/s. Combining fast video cameras, the magnetic pick-up arrays, and D_a monitors, it is found that an ELM is released once the pellet has penetrated about to the pedestal top. Generally, for the smallest pellets applied, the basic ELM signatures appeared to be rather similar to those of spontaneous ones. In contrast, larger pellets with deep penetration as applied in previous fuelling studies, tend to have a longer tail with larger integral particle loss, eventually followed by a cascade of several ELMs, though the ELM onset phase is not much different. The magnetic signature of a pellet induced ELM has been given already in figure 2 (right) in direct comparison with its spontaneous predecessor. With particle content of about $5 \cdot 10^{19}$ D-atoms, the injected pellet is already near the lower injector mass limit, but still penetrates well beyond the pedestal, depositing particles all along its path. Looking onto the top spectrogram in figure 2, there is no visible difference between both ELMs, except for the fact that the pellet triggered one is quickly followed by a second one, with clearly different precursor structure in between. Obviously, the pellet has changed the edge profile over its whole penetration depth, but still the released ELM, and hence the ELM affected area, seems to be not much different. After toroidal equilibration along field lines on a millisecond time scale, radial particle and energy transport into the depleted region continuously pushes up edge gradients and precursor mode activity, ultimately releasing a second ELM. The latter is quantitatively different, but otherwise

similar to a spontaneous one.

The detailed magnetic finger print of the pellet ELM (figure 2; bottom/right) still exhibits a few distinct differences to the spontaneous one. The maximum B_r values are about a factor of two higher (B_r scale scale indicated), there is no strong precursor mode, and the top and inside probes start earlier than the lfs probes. The latter is most probably due to the top-inside pellet seed perturbation, a helical plasmoid sheath, expanding along field lines and initiating the ELM [21]. On the lfs probes, we find a rather clear singular helical structure traveling again upward (6 km/s). However, inspection of a bunch of pellet ELMs shows usually a more complex poloidal mode structure, somewhere in between that of the presented pellet ELM and its spontaneous counterpart. In this context, we emphasize that with the present equipment, we have not yet reached the lower mass limit for prompt ELM release. Therefore, with further decreased pellet mass, we expect even less difference than described above.

5. Discussion

The combined experimental evidence described above may be summarized in terms of a spatio-temporal sequence of events and related physical mechanisms happening during an ELM cycle.

- Starting after a previous ELM, a surprisingly rich, finite amplitude inter-ELM and precursor mode activity is observed on magnetics, density and temperature in the pedestal region, with a wide range of (quasi-)mode numbers and frequencies. Intermediate n washboard-type modes rotating in the electron or ExB drift direction (opposite to the cross field mass rotation component) are one prominent example, another one are the low frequency perturbations seen by Thomson scattering and electron cyclotron emission.
- The initial, highly non-linear, electromagnetic ELM phase (~ 100 microseconds) is characterized by the rapid growth of a rather incoherent mix of modes, partly evolving from precursor modes and again with rotation in the electron drift direction.
- The following, still highly non-linear electromagnetic phase can be rather different probably because of progressive, highly variable 3d pedestal profile erosion as indicated by strong outer divertor D_α emission (the inner one delayed by an ion sound transit time). Incoherent broad band turbulence as well as semi-coherent modes, the latter even rotating in ion drift direction, have been observed.
- After several 100 microseconds from the ELM onset, the dB/dt signals die away, while their integrals, $B(t)$, still evolve, indicating some persistent 3d pedestal deformation in parallel to axisymmetric equilibrium shifts.

During the whole ELM (to some extent even in between ELMs), irregular filamentary structures, or bursts of structures, are observed in the scrape-off layer. Obviously, the highly perturbed pedestal region forms a quasi-continuous source of filaments drifting radially and decaying in amplitude due to parallel losses. Looking on the radial evolution of quasi-mode numbers, we find a clear trend from fairly low values, $n \leq 8$ in the pedestal, to 8-24 in the scrape-off layer and related divertor foot prints, and to even higher values at the limiter. Expressed in typical poloidal cross field wavelength, this means a change from typically half a meter in the pedestal down to centimeters at the limiter.

This spatio-temporal sequence suggests a qualitative interpretation in terms of a hierarchy of subsequent modes, which, in the absence of a comprehensive theoretical description, may be outlined in terms of a simplistic model, supported by published theory where available (e.g. the peeling-ballooning paradigm[23]). Starting after a preceding ELM crash, the pedestal pressure, and with some delay, the edge bootstrap current increase and micro-turbulence may

limit the gradient at a critical value. In parallel, intermediate modes, e.g. the observed washboard-type modes (possibly peeling/ballooning type), or tearing-type modes/islands may become linearly unstable, but saturate non-linearly, e.g. because of strong global magnetic shear. With some further rise in pressure gradient and especially edge current, these finite amplitude electromagnetic perturbations might grow and change character e.g. towards stronger ballooning at the lfs, where the local magnetic shear (essentially the radial variation of the magnetic pitch angle) is rather low, forming narrow helical ridges ('fingers' [24]) and, ultimately, detached filaments. Another more practical and roughly equivalent view of the same sequence is that a primary finite amplitude medium-n mode forms a new 3d toroidal-helical equilibrium, which becomes locally unstable to smaller scale ballooning modes, where toroidal and helical curvature add up. Since local shear (radial variation of magnetic pitch angle) is generally low at the lfs edge (apart from the bootstrap current distribution), these may eventually grow to very large amplitudes, split-off filaments, etc. This view is easily generalized to several rotating and interfering gross modes, with the most unstable secondary mode region still somewhere at lfs, but toroidally rotating. Notice that radial 'fingers' and certainly detached filaments should follow plasma mass rotation, as observed experimentally. The detailed filament detachment mechanisms are not easy to anticipate and must await more realistic models. But once detached, the parallel currents are limited by the ion saturation current at the wall intersections. The finite Langmuir sheath resistance there prevents full short circuit of the curvature driven charge separation current and keeps the filament radially drifting as qualitatively predicted by simple electrostatic models [20].

References

- [1] FEDERICI, G., et al., Plasma Phys. Controlled Fusion 45 (2003) 1523
- [2] SUTTROP, W., et al., Fusion Science & Techn. 44 (2003) 636
- [3] HORTON, L.D., et al., Nucl. Fusion 45 (2005) 856
- [4] LANG, P.T., et al., Nucl. Fusion 44 (2004) 665
- [5] LANG, P.T., et al., Nucl. Fusion 45 (2005) 502
- [6] KURZAN, B., et al., Phys. Rev.Lett. 95 (2005) 145001
- [7] NEUHAUSER, J., et al., Plasma Phys. Controlled Fusion 44 (2002) 855
- [8] NUNES, I., et al., Nucl. Fusion 44 (2004) 883
- [9] CONWAY, G.D., et al., Plasma Phys. Controlled Fusion 46 (2004) 951
- [10] BOLZONELLA, T., et al., Plasma Phys. Controlled Fusion 46 (2004) A143
- [11] MUELLER, H.W., et al., Profile and transport studies in the outer scrape-off layer at ASDEX Upgrade, 29th EPS conf., Montreux (Switzerland), ECA 26B (2002) O-2.06
- [12] KIRK, A., et al., Plasma Phys. Controlled Fusion 47 (2005) 995
- [13] HERRMANN, A., et al., Plasma Phys. Controlled Fusion 46 (2004) 971
- [14] HERRMANN, A., et al., The filamentary structure of ELMs in the scrape-off layer in ASDEX Upgerade, 17th PSI conf., Hefei (China), J.Nucl.Mater. subm.
- [15] EICH, T., et al., Phys. Rev. Lett., 91 (2003) 195003
- [16] EICH, T., et al., Plasma Phys. Controlled Fusion 47 (2005) 815
- [17] KURZAN, B., et al., 33th EPS conf., Rome (Italy), 2006, P2.132
- [18] BOBKOV, V., et al., Interaction of ICRH electric fields and the sol plasma in ASDEX Upgrade, 30th EPC conf., ECA 27A (2003) P-1.165
- [19] PEREZ, C.P., et al., Plasma Phys. Controlled Fusion 46 (2004) 61
- [20] KRASHENINNIKOV, S.I., Phys.Lett.A, 233 (2001) 368
- [21] LANG, P.T., et al., Czech.J.Phys. 55 (2005) 1557
- [22] LANG, P.T., et al., Plasma Phys. Controlled Fusion 48 (2006) A141
- [23] WILSON, H.R., et al., Phys. Plasmas 6 (1999) 1925
- [24] WILSON, H.R., COWLEY, S.C., et al., Phys. Rev. Lett., 92 (2004) 175006